Spin Transition in Magnesiowüstite in Earth's Lower Mantle

Taku Tsuchiya,[1,2,*] Renata M. Wentzcovitch,[1,2] Cesar R. S. da Silva,[2] and Stefano de Gironcoli[3,4]

[1]*Department of Chemical Engineering and Materials Science, University of Minnesota, Minnesota 55455, USA*
[2]*Minnesota Supercomputing Institute for Digital Technology and Advanced Computations, University of Minnesota, Minnesota 55455, USA*
[3]*Scuola Internazionale Superiore di Studi Avanzati, Trieste 34014, Italy*
[4]*DEMOCRITOS National Simulation Center, Trieste 34014, Italy*

(Received 22 September 2005; published 18 May 2006)

Iron in the major lower mantle (LM) minerals undergoes a high spin (HS) to low spin (LS) transition at relevant pressures (23–135 GPa). Previous failures of standard first principles approaches to describe this phenomenon have hindered its investigation and the clarification of important consequences. Using a rotationally invariant formulation of LDA + U we report a successful study of this transition in low solute concentration magnesiowüstite, $(Mg_{1-x}Fe_x)O$, ($x < 0.2$), the second most abundant LM phase. We show that the HS-LS transition goes through an insulating (semiconducting) intermediate mixed spins (MS) state without discontinuous changes in properties, as seen experimentally. We show that the HS state crosses over smoothly to the LS state passing through an insulating MS state where properties change continuously, as seen experimentally.

DOI: 10.1103/PhysRevLett.96.198501 PACS numbers: 91.60.Pn, 75.30.Kz, 81.40.Rs

Magnesiowüstite (Mw), $(Mg_{1-x}Fe_x)O$, is believed to be the major mineral phase in Earth's lower mantle (LM) after ferrosilicate perovskite, $(Mg_{1-x}Fe_x)SiO_3$ (hereafter Pv) [1]. The effect of iron incorporation on the thermodynamic and elastic properties of these minerals is a crucial issue in mineral physics. High spin to low spin (HS-LS) transitions in iron have been observed by *in situ* x-ray emission spectroscopy (XES) and Mössbauer spectroscopy from 40 to 70 GPa in Mw [2,3] and from 70 and 120 GPa in Pv [4–6] at room temperature. This transition is accompanied by volume reduction [3] and changes in these minerals' optical absorption spectrum. These can produce seismic velocity anomalies, variations in Mg-Fe^{2+} partitioning between Mw and Pv, changes in radiative heat conductivity, and compositional layering [2,4,7,8]. The elastic signature of this transition has now been partially explored [3], but there is still much to be quantified to pin down the effects of this spin transition on these properties. At the same time, the strongly correlated behavior of iron oxide has deterred the quantification of these changes by density functional calculations based on the local spin density (LSDA) and spin polarized generalized gradient approximations (σ-GGA). These approaches [9] produce incorrectly a metallic HS ground state and then successive spin collapses across the transition [10,11].

Here we use a rotationally invariant version of the local density approximation + Hubbard U (LDA + U) approach implemented in the plane wave pseudopotential method, where U is calculated in an internally consistent way [12]. This approach has been very successful in describing the electronic and structural properties of FeO, wüstite, under pressure [12], an antiferromagnetic insulator with a Néel temperature of 198 K. Details about the total energy calculations and pseudopotentials used here are reported in Ref. [13]. Most of our calculations were performed in 64-atoms supercells, but two calculations were also carried out in 128 and 216 atom supercells for convergence tests. We investigated Mw with $X_{Fe} =$ 3.125%, 12.5%, and 18.75%, the latter being similar to the experimentally investigated concentration, 17% [2,3]. The atomic configurations were ordered and homogeneous with Fe^{2+}s positioned as far from each other as possible. All atomic positions were completely relaxed in these LDA + U calculations. The Hubbard U was computed from the inverse density response matrices (interacting and noninteracting) obtained by applying localized potential shifts on single Hubbard sites [12]. Supercell size effects on U were estimated by using elements of the small density response matrices (from 64 atom supercells in all cases but also from 128 and 216 for) to construct response matrices corresponding to 512 atom supercells. This procedure [12] nicely captures size effects on U.

Us computed as functions of pressure for these three concentrations are shown in Fig. 1. They are approximately concentration independent for X_{Fe}s up to 18.75%. The increase of Us with pressure does not reflect an increase in correlation strength. First, Us and their pressure derivatives depend on the definition of the strongly correlated orbitals. We have used atomic like d-(pseudo)orbitals but other definitions are also possible [14]. Despite this nonuniqueness, total energies are always computed consistently using the same orbitals employed in the derivation of U, and their changes are physically meaningful. Second, in the Hubbard model it is the ratio U/Δ, where Δ is the d bandwidth, that characterizes the correlation strength, $U/\Delta \gg 1$ ($U/\Delta \ll 1$) corresponding to the strong (weak) correlated limit. For $X_{Fe} = 12.5\%$, $\frac{1}{\Delta}\frac{d\Delta}{dP}$ is $\sim$0.01, which is approximately 1 order of magnitude larger than $\frac{1}{U}\frac{dU}{dP}$, indicating, as expected, a decrease of correlation with pressure. Finally, the intermediate $S = 1$ spin state was never stabi-

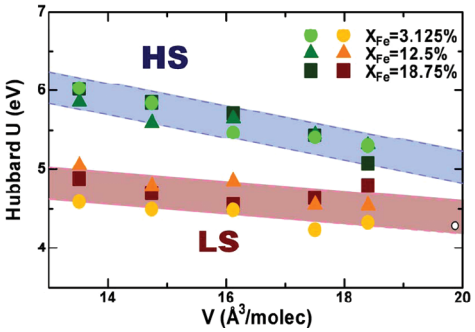

FIG. 1 (color). Computed Hubbard U as function of pressure for ferromagnetic HS and LS states. Us for antiferromagnetically ordered spins fall within these same ranges. $U_{HS} = -[0.15V - 7.92] \pm 0.2$ eV and $U_{LS} = -[0.06V - 5.61] \pm 0.2$ eV, where V is the volume per formula unit in Å [3]. Variations of U within these ranges have minor influence on the structural properties. Open circle is U for HS iron in FeO [12].

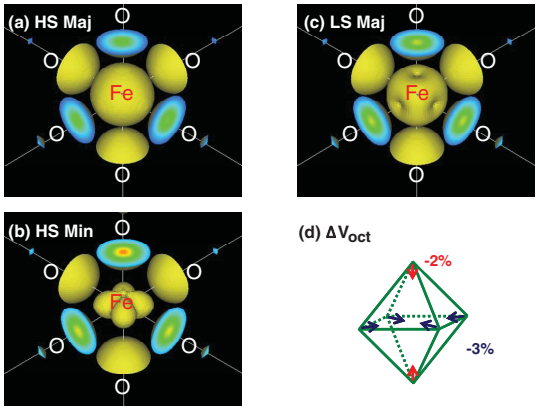

FIG. 2 (color). Pseudocharge densities around ferrous iron in Mw with $X_{Fe} = 12.5\%$. These are isosurfaces with $\rho = 0.3$ e/Å^3 for majority (a) and minority HS (b), and majority and minority LS (c). Depiction of the polyhedral volume collapse across the spin transition (d). Six caps surrounding the ferrous ion belong to oxygens.

lized in a self-consistent cycle, regardless of the initial occupation of iron d orbitals. The final stable state was always found to have $S = 0$ or 2, depending on pressure.

The electronic structure of Mw within the LDA + U approach is drastically different from that obtained using conventional LSDA [both as reported in Ref. [13] Figs. 1(a), (b)]. LDA + U produces the expected orbital occupancy of five majority electrons (three t_{2g} and two e_g) and one minority electron (t_{2g}). For $X_{Fe} = 12.5\%$, this results in a tetragonal Jahn-Teller distortion at the iron site associated with a 3 eV gap within the minority t_{2g} manifold. LDA + U also increases hybridization between majority $3d$ states and O$2p$ states, similar to the case of wüstite [12]. The latter indicates the insulating state has a moderate charge transfer character. For LS Mw, LDA + U opens a gap of approximately 2.6 eV between t_{2g} and e_g states without breaking the cubic symmetry. Although more information regarding the oscillation strength for electronic excitations is necessary, the moderate charge transfer gaps for both HS and LS Mw suggest that the optical absorption spectrum of Mw should display a redshift across the spin transition, not a blueshift as estimated by simple crystal field arguments [2,15].

Some of the effects described here are captured in Fig. 2, which shows the total pseudocharge density contours around the ferrous ion in Mw. Figs. 2(a) and 2(b) show majority and minority HS densities, respectively, and Fig. 2(c) shows majority and minority LS densities. The majority charge in HS iron is nearly spherical, while the minority charge shows only one occupied t_{2g} state. The Jahn-Teller distorted HS state expands the octahedral x and y axes by 2% and the z axis by 1%. The charge density contour of the LS state shows a smaller ferrous iron with cubic symmetry. Replacement of magnesium by LS iron shrinks the octahedral edges uniformly by 1%. Therefore, this spin transition induces the octahedral volume reduction of 8%, shown in Fig. 2(d). These effects indicate that the electronic structure and the change in internal energy involved in the spin transition of Mw should not be addressed using simple crystal field considerations [2,4,8,9].

The dependence of the transition pressure, P_t, on X_{Fe} has been investigated experimentally across the entire range of compositions in this isomorphous alloy [3,16]. It has been shown that P_t increases with X_{Fe} in high-concentration Mw ($X_{Fe} > 25\%$). Figure 3(a) shows the enthalpy differences between the LS and HS states ($\Delta H_{LS\text{-}HS}$) obtained in static calculations for three different concentrations. Within our accuracy and for these small values of X_{Fe}, the transition pressure (P_t) is 32 ± 2 GPa and does not depend on X_{Fe}. This result implies that chemical, exchange, and elastic interactions between neighboring irons are negligible in low-concentration Mw. Therefore, up to $X_{Fe} = 18.75\%$, a particular HS iron should undergo the spin transition at the same P_t, irrespective of the state of neighboring irons, be they LS or HS, parallel or antiparallel. This implication is verified in Fig. 3(b), which shows the difference in enthalpy, ΔH, in $X_{Fe} = 18.75\%$ Mw between states with various fractions of coexisting LS and HS irons, represented by $n = n_{LS}/(n_{HS} + n_{LS})$. This implies that at 0 K and up to $X_{Fe} = 18.75\%$, the spin transition is sharp and should be approximately concentration independent, as shown in Fig. 3(a). In addition, it points to the possibility of the high temperature stabilization of a mixed spin (MS) state by an increase in HS-LS configuration entropy, $S_{LS\text{-}HS}$.

Static compression curves for $X_{Fe} = 18.75\%$ in various MS states are shown in Fig. 3(c) along with measurements at room temperature in 17% iron Mw [3]. The latter changes smoothly ($54 < P_t < 67$ GPa) and spans the predicted compression curves of $0 < n < 1$. This appears to be evidence of a continuous increase in LS fraction, n, that could originate in pure thermodynamic equilibrium, as indicated by our calculations. The wide transition pressure range could also have a contribution from hysteresis, since there are large octahedral volume changes associated with

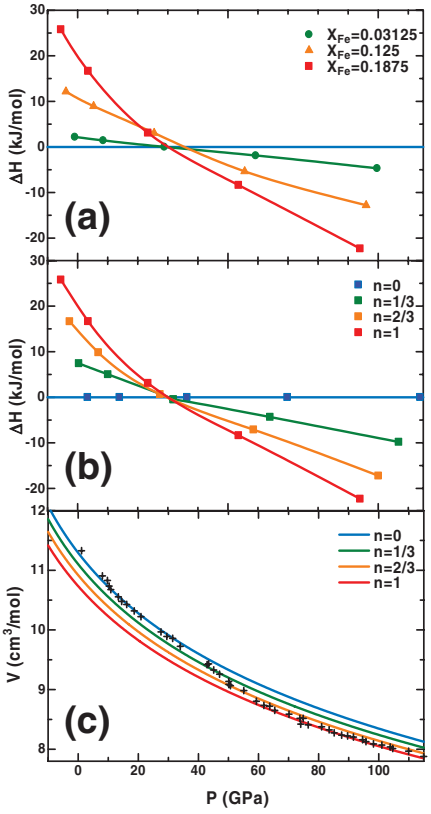

FIG. 3 (color). Static enthalpy differences between LS and HS phases at three different iron concentrations (a). Enthalpy differences in Mw with $X_{\mathrm{Fe}} = 18.75\%$, between states with various fractions of coexisting HS and LS irons, $n = n_{\mathrm{LS}}/(n_{\mathrm{HS}} + n_{\mathrm{LS}})$, and the HS state (b). The reference green line corresponds to the enthalpy of all irons in the HS state ($n = 0$). Pressure-volume curves for the same ns (c) shown in (b). Experimental results [3] at 300 K for Mw with $X_{\mathrm{Fe}} = 17\%$ are represented by $+$.

the transition. Experiments at higher temperatures should distinguish these effects: hysteresis should decrease the transition pressure range with temperature, thermodynamic equilibrium should increase the same. Experimental and theoretical compression curves of the initial HS and final LS states also agree quite well below ~40 GPa (HS state) and above ~60 GPa (LS state). The slight underestimation of calculated volumes at low pressures is typical of static calculations lacking zero point motion and thermal effects at 300 K. Up to $X_{\mathrm{Fe}} = 18.75\%$; we find the zero pressure equilibrium volume, V_0, in the HS state increases linearly with $dV_0/dX_{\mathrm{Fe}} = 10.5 \times 10^{-3}\ \mathrm{cm}^3/\mathrm{mol}$, consistent with experimental observations, $dV_0/dX_{\mathrm{Fe}} = 8.9 \times 10^{-3}\ \mathrm{cm}^3/\mathrm{mol}$ [17]. The zero pressure bulk modulus, $dB_0/dX_{\mathrm{Fe}} = 0.28$ GPa for HS Mw and 1.06 GPa for LS Mw, also increases and is in good agreement with the quite X_{Fe}-insensitive B_0 measured for HS Mw [17]. A considerable volume reduction of 4.2% can be seen across the spin transition at $X_{\mathrm{Fe}} = 18.75\%$ in Fig. 3(c). For $X_{\mathrm{Fe}} \leq 18.75\%$, this volume reduction is linear in X_{Fe} and in n, and can be represented by $d\Delta V/dX_{\mathrm{Fe}} = -2.22 \times 10^{-2} n X_{\mathrm{Fe}}\ \mathrm{cm}^3/\mathrm{mol}$. An increase in bulk modulus from 297 to 313 GPa is seen at $X_{\mathrm{Fe}} = 18.75\%$ and at the static transition pressure. Similar to the volume change, the change in B_0 can be expressed as $d\Delta B/dX_{\mathrm{Fe}} = 0.84 n X_{\mathrm{Fe}}$ GPa.

So far, only static results have been discussed. Phase boundary calculations require knowledge of entropies and Gibbs free energies at arbitrary temperatures for all relevant states. The first important contribution to the entropy is the magnetic one:

$$S_{\mathrm{mag}} = k_B X_{\mathrm{Fe}} (1 - n) \ln[m(2S + 1)], \qquad (1)$$

where k_B is the Boltzmann constant, S is the iron spin quantum number ($S = 2$ for HS and $S = 0$ for LS), n is the LS iron fraction, and m is the electronic configuration degeneracy (for the minority HS t_{2g} orbitals, $m = 3$; for LS $m = 1$) [18]. The second contribution is the configuration entropy for coexisting HS and LS irons:

$$S_{\mathrm{conf}} = -k_B X_{\mathrm{Fe}} [n \ln n + (1 - n) \ln(1 - n)], \qquad (2)$$

(HS and LS irons are like different chemical species). The vibrational entropies of the HS, LS, and MS states should be similar and we neglect their differences, even though this effect should still be investigated at some point. It is also reasonable to neglect at this point the difference in Fe/Mg configuration entropy between various spin states.

With these assumptions, the Gibbs free-energy can be minimized with respect to the LS fraction n to give

$$n = \frac{1}{1 + m(2S + 1) \exp\left\{\frac{\Delta H_{\mathrm{LS\text{-}HS}}(P)}{k_B X_{\mathrm{Fe}} T}\right\}},$$

where $\Delta H_{\mathrm{LS\text{-}HS}} = (H_{\mathrm{LS}}^{\mathrm{stat}}(P) - H_{\mathrm{HS}}^{\mathrm{stat}}(P))$ is the difference between the static enthalpies of LS and HS states shown in Figs. 3(a) and 3(b). Details of this derivation are presented in Ref. [13], while the plot of $n(P, T)$ in Mw with $X_{\mathrm{Fe}} = 18.75\%$ is shown in Fig. 4. This is close to the concentration relevant for the lower mantle. A mantle geotherm [19] is displayed in Fig. 4 also for reference. It can be seen that no sharp discontinuous changes in n, therefore in structural or optical properties, should be expected to occur across this spin crossover in the mantle. This might start at the top of the lower mantle and continue down to and beyond the core-mantle boundary (135 GPa and ~4000 K). This is probably the most important consequence of these results for our understanding of the lower mantle. Phonon renormalization of U might alter this picture at the highest temperature and lower pressures. The difference between our crossover pressure range at 300 K and the experimental ranges might result from (a) our neglect of differences in vibrational and Mg/Fe configurational entropies between various states considered, (b) uncertainties in the total energy related to uncertainties in Us, (c) neglect of configurations containing second neighbor irons, since iron-iron interactions increase P_t (see below); (d) it could also result from some hysteresis present in experiments, whose transition pressure ranges differ somewhat from each other as well.

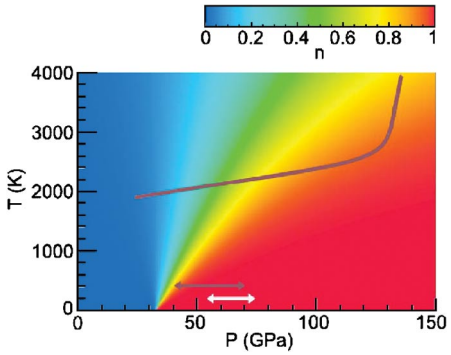

FIG. 4 (color). Spin cross over in Mw with $X_{Fe} = 18.75\%$. n is the fraction of LS irons. Experimental transition pressures at 300 K in Mw with $X_{Fe} = 17\%$ are from x-ray emission spectroscopy. They are denoted by gray [2] and white [3] arrows, respectively. The gray line is a lower mantle geotherm [20]. For reference, the melting temperature of MgO at ambient pressure is ~3100 K increasing to ~4000 K at ~33 GPa [25].

The behavior of Mw for $X_{Fe} > 18.75\%$ could not be easily addressed. Iron-iron interactions are no longer negligible and P_t becomes strongly dependent of concentration and on magnetic state. For instance, in Mw with $X_{Fe} = 25\%$ we identified a tendency for structural ordering, antiferromagnetic alignment, and we found $P_t > 125$ GPa. This tendency parallels experimental observations in Mw with $X_{Fe} = 60\%$, where $84 < P_t < 102$ GPa[3] and with $X_{Fe} = 100\%$, where no spin transition up to 143 GPa [16] has been reported. A similar calculation in FeO has not found any spin transition up to 300 GPa either [20]. Mw with $X_{Fe} = 50\%$ and 60% were also reported to dissociate into iron reach and iron poor phases [21], a clear consequence of iron-iron interactions. These interactions, that involve cooperative Jahn-Teller distortions and orbital ordering [12], prevented us from extending our low-solute concentration treatment to higher concentrations. Although X_{Fe} in Mw in the LM is expected to be ~20%, iron partitioning between Mw and Pv could be affected by the spin transition [2,4]. Our current understanding of this multiphase/multicomponent system is too limited to allow us to speculate on its equilibrium state at LM conditions. However, the Gibbs free-energy difference between HS and LS Mw, $\Delta G_{HS\text{-}LS}$ increases rapidly with pressure (see Ref. [13], Fig. 2), suggesting iron prefers to partition more towards Mw with increasing pressure, in the low-concentration regime. This is also suggested by recent experiments in realistic compositions like peridotite [22]. The spin transition in Pv and in its high-pressure form, post-perovskite [23,24], should also affect the equilibrium concentrations. Unfortunately, not enough quantitative information is available about these systems yet.

In summary, the pressure induced spin transition in a strongly correlated iron-bearing mineral is successfully described by a first principles approach. In Mw, the pressure induced HS-LS transition is direct from insulating $S = 2$ to $S = 0$, is expected to display a red shift in the optical gap, and displays a slow crossover with respect to pressure at high temperatures. No sharp changes in optical or elastic properties of Mw should be expected across the lower mantle, unless, perhaps if X_{Fe} increases beyond ~20%. For higher solute concentrations, interactions between irons leading to complex ordering phenomena may occur [21,26].

We acknowledge J. Tsuchiya and P. B. Allen for stimulating discussions. R. M. W. is grateful to the Department of Geosciences at Stony Brook University for hospitality during the revision stages of this research. Research was supported by NSF Grants No. EAR-0135533, No. EAR-0230319, No. ITR-0325218 (ITAMIT), No. ITR-0428774 (***VLab***), and No. DMR-0212302 (U. of Minnesota MRSEC).

*Present address: Geodynamics Research Center, Ehime University, 2-5 Bunkyo-cho, Matsuyama 790-8577, Japan.

[1] G. R. Helffrich and B. J. Wood, Nature (London) **412**, 501 (2001).
[2] J. Badro *et al.*, Science **300**, 789 (2003).
[3] J.-F. Lin *et al.*, Nature (London) **436**, 377 (2005).
[4] J. Badro *et al.*, Science **305**, 383 (2004).
[5] J. Li *et al.*, Proc. Natl. Acad. Sci. U.S.A. **101**, 14 027 (2004).
[6] J. M. Jackson *et al.*, Am. Mineral. **90**, 199 (2005).
[7] E. S. Gaffney and D. L. Anderson, J. Geophys. Res. **78**, 7005 (1973).
[8] D. M. Sherman, J. Geophys. Res. **96**, 14 299 (1991).
[9] W. Sturhahn *et al.*, Geophys. Res. Lett. **32**, L12 307 (2005).
[10] D. M. Sherman and H. J. F. Jansen, Geophys. Res. Lett. **22**, 1001 (1995).
[11] R. Cohen *et al.*, Science **275**, 654 (1997).
[12] M. Cococcioni and S. de Gironcoli, Phys. Rev. B **71**, 035105 (2005).
[13] See EPAPS Document No. E-PRLTAO-96-016621 for details about the total energy calculations and pseudopotentials. For more information on EPAPS, see http://www.aip.org/pubservs/epaps.html.
[14] S. Fabris *et al.*, Phys. Rev. B **71**, 041102 (2005).
[15] R. G. Burns,. *Mineralogical Application of Crystal Field Theory* (Cambridge University Press, Cambridge, England, 1993).
[16] J. Badro *et al.*, Phys. Rev. Lett. **83**, 4101 (1999).
[17] S. D. Jacobsen *et al.*, J. Geophys. Res. **107**, 2037 (2002).
[18] H. H. Ulbrich and D. R. Waldbaum, Geochim. Cosmochim. Acta **40**, 1 (1976).
[19] R. Boehler, Rev. Geophys. **38**, 221 (2000).
[20] S. Gramsch *et al.*, Am. Mineral. **88**, 257 (2003).
[21] L. S. Dubrovinski *et al.*, Science **289**, 430 (2000).
[22] M. Murakami *et al.*, Geophys. Res. Lett. **32**, L03304 (2005).
[23] M. Murakami *et al.*, Science **304**, 855 (2004).
[24] T. Tsuchiya *et al.*, Earth Planet. Sci. Lett. **224**, 241 (2004).
[25] A. Zerr and R. Boehler, Nature (London) **371**, 506 (1994).
[26] Speziale *et al.*, Proc. Natl. Acad. Sci. U.S.A. **102**, 17 918 (2005).